MAX-PLANCK-INSTITUT FÜR PLASMAPHYSIK

GARCHING BEI MÜNCHEN

Collapse of Alfvén Modes into Ballooning-Type Modes due to Toroidal Nonaxisymmetry

A. SALAT

IPP 6/305 November 1991

Die nachstehende Arbeit wurde im Rahmen des Vertrages zwischen dem Max-Planck-Institut für Plasmaphysik und der Europäischen Atomgemeinschaft über die Zusammenarbeit auf dem Gebiete der Plasmaphysik durchgeführt.

Abstract

The effect of nonaxisymmetry on Alfvén modes in toroidal geometry is investigated numerically. A model equation is used which simplifies the analysis on the resonant surfaces. Alfvén modes, characterized by their poloidal and toroidal node numbers (m, n), are found to exist in moderate nonaxisymmetry as well. For fixed (m, n), however, the mode collapses from a global feature on the resonant surface into an infinitely thin Alfvén ballooning mode along a field line if the nonaxisymmetry exceeds a critical threshold or, with given nonaxisymmetry, if the poloidal variation does so. Alfvén balloonings are polarized within the magnetic surfaces and are stable.

1. Introduction

The aim of this study is to demonstrate numerically the collapse of global Alfvén modes on resonant surfaces of a nonaxisymmetric plasma torus into localized (Alfvén) ballooning-type modes if the nonaxisymmetry is increased above a critical threshold or, with fixed nonaxisymmetry, if the variation of the plasma equilibrium on a poloidal cross-section becomes too large.

In order to put the result into perspective, a short review of the MHD continuum in simple geometry may be useful.

A homogeneous plasma in a constant magnetic field $\mathbf{B}$ according to ideal MHD theory supports three types of waves: Alfvén waves, slow waves and fast waves; see, for example, [1]. Assuming the waves to be space and time dependent as $\sim \exp[i(\mathbf{k}\cdot\mathbf{r}+\omega t)]$, the dispersion relation of Alfvén waves is

$$(\,\mathbf{k}\cdot\mathbf{B}\,)^2 \;-\; \omega^2\,\rho \;=\; 0\;, \tag{1.1}$$

where ρ is the plasma mass density. Since (shear) Alfvén waves, in contrast to slow and fast waves, do not involve plasma compression, their dispersion relation, equ. (1.1), is particularly simple, and we shall be concerned with the other two types only in passing.

In an inhomogeneous plasma the value ω given by equ. (1.1) splits into a continuum of resonances. An example is a straight plasma cylinder with smooth radial profiles. In cylindrical coordinates r, θ, z, with the ansatz $\boldsymbol{\xi} = \mathbf{a}(r)\,\exp[\,i(m\theta + k_z z + \omega t)\,]$ for the plasma displacement $\boldsymbol{\xi}$, etc., one obtains an ODE [2], [3],

$$\frac{\mathrm{d}}{\mathrm{d}r}\,[\;f(\omega,r)\;\frac{\mathrm{d}}{\mathrm{d}r}\;(r\;a_r)\;]\;-\;g(\omega,r)\;a_r(\omega,r)\;=\;0\;, \tag{1.2}$$

for the radial component a_r of $\mathbf{a}$. The quantities f, g and a_r all depend parametrically on m and k_z. Equation(1.2) becomes singular where $f(\omega,r)=0$. f is of the form

$$f(\omega,r) \;=\; [\,(\,\mathbf{k}\cdot\mathbf{B}\,)^2 \;-\; \omega^2\,\rho\,]\;[\,\gamma P\,(\,\mathbf{k}\cdot\mathbf{B}\,)^2 \;-\; \omega^2\,\rho\,(\,\gamma P \;+\; B^2\,)\,]\;f_1(\omega,r)\;, \tag{1.3}$$

with f_1 finite where the prefactors vanish. Here $\mathbf{k}\cdot\mathbf{B} = m\,B_\theta + k_z\,B_z$, γ is the ratio of specific heats and P is the plasma pressure. Singularity therefore occurs where the dispersion relation (1.1) is satisfied, i.e. for Alfvén waves, or where the second square brackets vanish, i.e. for slow waves. Since $\mathbf{B} = \mathbf{B}(r)$, there are two corresponding

continua of frequencies $\omega = \omega(r)$. For fixed ω, a_r has a logarithmic singularity at the resonant surfaces r_ω, while a_θ and a_z diverge as $(r - r_\omega)^{-1}$.

A knowledge of continua in the spectrum, apart from its intrinsic interest, is important for practical purposes. If instead of a Fourier ansatz $\sim \exp(i\omega t)$ an initial value problem is considered, a continuum gives rise to a collective plasma motion, called quasimode, which is damped by phase mixing [4]. This damping increases the absorption of externally launched waves and is the basis of, for example, Alfvén wave heating of fusion plasmas [5]. The present investigation contributes to the understanding of the continuum in general toroidal geometry.

The term $\mathbf{k} \cdot \mathbf{B}$ in equs. (1.1), (1.3) is equivalent to the operator $\mathbf{B} \cdot \nabla$. This operator governs the continuous spectrum in toroidal geometry as well; see [3], [6] for the axisymmetric case, and [7], [8], [9] and [10] for the general case. In contrast to the algebraic equations for $\omega = \omega(r)$ above, those values of $\omega = \omega(\psi)$ for which a system of *differential equations* $\mathrm{H}(\mathbf{B} \cdot \nabla,\ \omega,\ \psi) \cdot \mathbf{X} = 0$, equs. (2.3) or (2.5), has bounded single-valued solutions on the magnetic surfaces $\psi = const$ are in the continuous spectrum (or in a dense point spectrum; see below). The equations act purely within the surfaces, with ψ being a parameter only. In addition, it must be shown that the *full* system of mode equations has a singularity in the radial direction, i.e. in the ψ-direction, at the resonant surfaces.

The operator $\mathbf{B} \cdot \nabla$ has two different aspects. Let θ and ϕ be poloidal and toroidal coordinates, respectively. With $B^\theta = \mathbf{B} \cdot \nabla\theta$, $B^\phi = \mathbf{B} \cdot \nabla\phi$, the operator $\mathbf{B} \cdot \nabla = B^\theta\, \partial/\partial\theta + B^\phi\, \partial/\partial\phi$, on the one hand, is a partial differential operator on the surfaces spanned by $0 \leq \theta,\ \phi \leq 2\pi$. On the other hand, $\mathbf{B} \cdot \nabla = B\mathrm{d}/\mathrm{d}s$ can be viewed as an ordinary derivative with respect to the arc length s along $\mathbf{B}$. This implies that the behaviour in cases with closed field lines may differ from ergodic cases. Here, we consider only surfaces with ergodic field lines.

In the context of the first aspect the natural boundary conditions are periodicity of the solution $\mathbf{X}(\theta, \phi)$ of equ. (2.5) in θ and ϕ. In axisymmetric geometry such solutions exist, namely the modes from the Alfvén continuum [3], [6]. At fixed ψ, they may be uniquely labelled by two discrete parameters m and n. The continuous spectrum therefore consists of the union of all $\omega = \omega_{m,n}(\psi)$. With respect to the radial variable ψ, at fixed ω, there is a singularity at the resonant surface $\psi = \psi(\omega)$. In the following it is shown numerically, this being supported by theory, that these doubly periodic solutions $\mathbf{X}(\theta, \phi)$ continue to exist also in weakly *nonaxisymmetric* toroidal geometry. They may still be labelled by two parameters m and n. The full analogy to the axisymmetric case

indicates that the necessary ingredient for the Alfvén continuum, a singularity in ψ, is also present. We do not investigate the singularity behaviour further, however. Instead, we concentrate on the properties of the differential equation $\mathrm{H}(\mathbf{B}\cdot\nabla,\ \omega,\ \psi)\cdot\mathbf{X}=0$ itself, which refers solely to the behaviour *within* the magnetic surfaces.

It turns out, however, that if the nonaxisymmetry becomes too strong, or, with fixed nonaxisymmetry, if the poloidal variations become too large, any particular mode (m,n) ceases to exist. Instead of global modes, equ. (2.5) develops solutions $\mathbf{X}=\mathbf{X}(s)$ which are defined only locally, along single field lines. Thus, the second aspect of $\mathbf{B}\cdot\nabla$ mentioned above becomes dominant. It is found that along the field line the amplitude falls off exponentially on both sides of a maximum, with finite localization length. Across the field line, however, the localization is infinitely strong. The modes are therefore singular also *within* the magnetic surfaces and are of a ballooning-type character.

The paper is organized as follows: in Sec. 2 the differential equations for the MHD spectrum in general toroidal geometry are reviewed as far as is relevant for the present purposes. Owing to the combined poloidal and toroidal modulation of the MHD equilibrium they have coefficients with quasiperiodic dependence along the field lines. Instead of the exact equation for $\mathbf{X}(\theta,\phi)$ or $\mathbf{X}(s)$ a simplified model equation is introduced in Sec. 3. In addition, the smooth dependence of the equilibrium quantities is replaced by a discrete model.

In Sec. 4 pertinent results from the theory of quasiperiodic differential equations are discussed and numerical results showing the catastrophic transition from global to local character of the modes are presented. A discussion and conclusions are given in Sec. 5.

2. MHD spectrum and quasiperiodicity

As is usual in this context, we assume the existence of nonaxisymmetric toroidal MHD equilibria with nested magnetic surfaces $\psi = const.$ (A comment on this is given below in Sec. 5.) The linearized MHD equations [1], with the ansatz $\sim \exp(i\omega t)$, may then be put into the instructive form [7]

$$\begin{aligned} \frac{\partial \mathbf{S}}{\partial \psi} &= \mathrm{A}\cdot\mathbf{S} + \mathrm{C}\cdot\mathbf{R}\,, \\ \mathrm{H}\cdot\mathbf{R} &= \mathrm{K}\cdot\mathbf{S}\,, \end{aligned} \tag{2.1}$$

where $\mathbf{S}$ and $\mathbf{R}$ are vectors defined by

$$\mathbf{S} = \begin{pmatrix} v^1 \\ p^* \end{pmatrix}\,, \qquad \mathbf{R} = \begin{pmatrix} v^2 \\ v^3 \\ b^2 \\ b^3 \end{pmatrix} \tag{2.2}$$

and A, C, H, K are matrix operators whose elements contain derivatives within the magnetic surfaces only. In equs. (2.2) $v^i = \mathbf{v}\cdot\nabla r^i$, $i = 1,\ 2,\ 3$, are the contravariant components of $\mathbf{v} = i\omega\boldsymbol{\xi}$ with respect to the coordinates $(r^1, r^2, r^3) = (\psi, \theta, \phi)$, etc. Furthermore, $p^* = p + \mathbf{B}\cdot\mathbf{b}$, where p and $\mathbf{b}$ are the perturbations of the pressure and magnetic field respectively, and $\boldsymbol{\xi}$ is the plasma displacement.

If the operator H has an inverse, for given $\omega = \omega_0$ and $\psi = \psi_0$, then equs. (2.1) may be integrated across $\psi = \psi_0$. However, if the inverse does not exist, i.e. if for some $\omega = \omega_0$ and $\psi = \psi_0$ there is a nontrivial vector function $\mathbf{X}$, defined on the surface ψ_0, such that

$$\mathrm{H}\cdot\mathbf{X}(\theta,\phi) = 0\,, \tag{2.3}$$

then solutions singular for $\psi \to \psi_0$ may exist. The proof of their existence is done by, for example, Taylor expansion of the operators A etc. around $\psi = \psi_0$, and an ansatz like

$$\begin{aligned} \mathbf{R} &= (\psi-\psi_0)^{-1}\,[\,\hat{\mathbf{X}}_0(\theta,\phi) + \cdots] + \ln(\psi-\psi_0)\,[\,\mathbf{U}_0(\theta,\phi) + \cdots]\,, \\ \mathbf{S} &= \ln(\psi-\psi_0)\,[\,\hat{\mathbf{Y}}_0(\theta,\phi) + \cdots] + \mathbf{V}_0(\theta,\phi) + \cdots\,, \end{aligned} \tag{2.4}$$

where the higher-order terms $\cdots$ contain positive powers of $\psi-\psi_0$ multiplied by functions of θ and ϕ. Alternatively, an ansatz with leading powers $(\psi-\psi_0)^\nu$ and $(\psi-\psi_0)^{\nu+1}$

for $\mathbf{R}$ and $\mathbf{S}$, respectively, is possible. In this case $\nu < 0$ or ν complex indicates singularity. To lowest order in $\psi - \psi_0$ the relation $\mathrm{H}_0 \cdot \hat{\mathbf{X}}_0 = 0$ is recovered. Higher-order equations are solved recursively. This approach to the continuum works well in the axisymmetric case [3], [6]. In nonaxisymmetry this kind of proof of a radial singularity, in spite of attempts, has not been worked out so far: see [7], [8], [11]. Nevertheless, equ. (2.3) is a prerequisite for the Alfvén (and slow-mode) continuum and will be investigated in the following.

A coordinate-independent form of equ. (2.3), valid if $\mathbf{J} = \mathrm{curl}\ \mathbf{B}$ is not parallel to $\mathbf{B}$, is obtained by elimination of b^2, b^3 [8]:

$$[\ \mathbf{B}\cdot\nabla\ \mathrm{M}\ \mathbf{B}\cdot\nabla\ +\ \omega^2\ \rho\ \mathrm{N}\ ]\cdot\hat{\mathbf{X}}\ =\ 0\ , \tag{2.5}$$

where

$$\mathrm{M}\ =\ \begin{pmatrix} \gamma P\ \mathbf{B}\cdot\mathbf{B}\ /\ B_* & \gamma P\ \mathbf{B}\cdot\mathbf{J}\ /\ B_* \\ \gamma P\ \mathbf{B}\cdot\mathbf{J}\ /\ B_* & \mathbf{J}\cdot\mathbf{J}\ -\ (\mathbf{B}\cdot\mathbf{J})^2\ /\ B_* \end{pmatrix}\ , \tag{2.6}$$

$$\mathrm{N}\ =\ \begin{pmatrix} \mathbf{B}\cdot\mathbf{B} & \mathbf{B}\cdot\mathbf{J} \\ \mathbf{B}\cdot\mathbf{J} & \mathbf{J}\cdot\mathbf{J} \end{pmatrix}\ , \tag{2.7}$$

and $B_* = \gamma P + \mathbf{B}\cdot\mathbf{B}$. $\hat{\mathbf{X}} = (u,\ v)^T$ contains the coefficients u, v of the tangential components $\xi^i = u\,B^i + v\,J^i$, $i =\ 2,\ 3$, of the displacement vector.

In the spectral theory of linear operators consideration of the continuous spectrum is often extended to the essential spectrum. In addition to the continuum, it also comprises, for example, dense sets of eigenvalues and eigenvalues of infinite multiplicity; see, for example, [12]. A necessary and sufficient condition for ω to be in the essential spectrum of a selfadjoint linear operator L is the existence of a normed singular sequence of approximate eigenfunctions $\{Z_\epsilon\}$, $\|Z_\epsilon\| = 1$, such that $\|(\mathrm{L} - \omega)\,Z_\epsilon\| \to 0$ for $\epsilon \to 0$, and such that the sequence contains no convergent subsequence.

In the MHD case Z corresponds to the union of $\mathbf{R}$ and $\mathbf{S}$. The sequence of Z_ϵ can, for example, be a sequence of functions localized more and more in normal direction around a fixed $\psi = \psi_0$. This type of approach has been used in, for example, [3] and [10] for the axisymmetric case. Hameiri [10] extended it to the general toroidal case but for ballooning-type modes only. They correspond to a singular sequence which for $\epsilon \to 0$ contracts onto a *single field line*. Two types of ballooning are considered in [10]:
1. Ballooning modes proper, with displacement $\boldsymbol{\xi}$ and field perturbation $\mathbf{b}$ having a normal component *out of* the magnetic surfaces. They are the analoga of the classical

ballooning modes on closed field lines, as considered in, for example, [13], [14] and [15]. Localization with $\epsilon \to 0$ is stronger within the surfaces than in the normal direction. 2. Modes for which $\boldsymbol{\xi}$ and $\mathbf{b}$ lie *within* the surfaces, for $\epsilon \to 0$. The localization is stronger in the normal than in the tangential direction. They are described [10] by the same equations as the global Alfvén modes, e.g. equs. (2.5), except that M and N are considered functions of the arc-length s along a field line, instead of the angles θ and ϕ. One might call them Alfvén ballooonings. (Since $\boldsymbol{\xi}$ and $\mathbf{b}$ are *within* the surfaces, some other name, such as "stretching" modes, might be more apt than "ballooning" modes.) For ballooning-type modes we consider it a reasonable boundary condition that their amplitudes decrease to zero with a finite decay length L along the field line, for $s \to \pm\infty$. (Hameiri [10] admits the weaker condition $L(\epsilon) \to \infty$ for $\epsilon \to 0$, with the consequence that the whole magnetic surface may be covered more or less evenly by singularities. This incoherent structure is possibly of less physical significance than a ballooning-type mode with finite decay length.) In the following we investigate Alfvén and Alfvén ballooning modes together and do not consider type 1 ballooonings.

In *axisymmetric* toroidal geometry the ansatz $\sim \exp(in\phi)$ for global modes is possible. Equations (2.5) become ODEs in θ, with periodic coefficients, since the equilibrium is periodic in the poloidal angle (irrespective of whether the field lines are ergodic or not). From the Floquet theory of differential equations with periodic coefficients it follows that a one-parameter family of solutions with the period of the coefficients exists, distinguished by the node number, so that together with the parameter n there exists a two-parameter family of continuum modes on the surfaces $\psi = const$, as mentioned in the Introduction.

Alfvén ballooning (A. ballooning) modes do not exist in axisymmetry since linear equations with periodic coefficients, according to the Floquet theory, do not possess solutions which decay on both sides $s \to \pm\infty$.

We return to the general *nonaxisymmetric* toroidal case. A transform of variables is useful. First we transform to such angles θ, ϕ that the field lines are straight and B^θ and B^ϕ are constant on the magnetic surfaces [16]. Next we define coordinates x and y by setting

$$\theta = x\,, \qquad \phi = q\,x + y\,, \tag{2.8}$$

where $q = q_s \equiv B^\phi / B^\theta$ is the safety factor. Since we consider only ergodic field lines, q is an irrational number. One obtains

$$\mathbf{B} \cdot \nabla \;=\; B^\theta \left.\frac{\partial}{\partial x}\right|_y \;=\; B^\theta \frac{\mathrm{d}}{\mathrm{d}x} \,. \tag{2.9}$$

Thus, x, like s, is a coordinate along $\mathbf{B}$, while y parametrizes the field lines. $\mathrm{M}(\theta, \phi) = \mathrm{M}(x, qx + y)$, and analogously N, which are 2π-periodic in θ and ϕ, are therefore periodic with the same period in both x and qx. This property, for irrational q, is called quasiperiodicity. Equation (2.5) can therefore be viewed as a system of ordinary differential equations in x with quasiperiodic coefficients. In the next section we introduce a simplified model equation as a substitute for it.

3. Model equation

In the limit of small $\beta = \gamma P/(\gamma P + \mathbf{B}\cdot\mathbf{B}) \ll 1$ equ. (2.5) transforms to a scalar equation. With $[\mathbf{J}\times\mathbf{B}] = \nabla P = (\mathrm{d}P/\mathrm{d}\psi)\nabla\psi$, in agreement with [17], one easily obtains

$$\left[B^\theta \frac{\mathrm{d}}{\mathrm{d}x}\, a\, B^\theta \frac{\mathrm{d}}{\mathrm{d}x}\frac{1}{a} + \rho\,\omega^2 \right] U(x) = 0\,, \tag{3.1}$$

where

$$a(x) = \frac{(\nabla\psi)^2}{\mathbf{B}\cdot\mathbf{B}} \tag{3.2}$$

and $U = v/a$. The transition from two coupled equations to one scalar equation for U corresponds to the decoupling of the Alfvén continuum from the slow-mode continuum.

For the sake of simplicity and in order to have access to analytical results, we neglect the first-order derivative of U in equ. (3.1). The following model equation for the essential spectrum is obtained:

$$\left[\frac{\mathrm{d}^2}{\mathrm{d}x^2} + (\hat{\omega}^2 - V) \right] U(x) = 0\,, \tag{3.3}$$

where

$$\hat{\omega}^2 = \frac{\rho\omega^2}{(B^\theta)^2}\,, \tag{3.4}$$

and

$$V = -\frac{1}{B^\theta}\frac{\mathrm{d}}{\mathrm{d}x}\left(a\, B^\theta \frac{\mathrm{d}}{\mathrm{d}x}\frac{1}{a} \right)\,. \tag{3.5}$$

Equation (3.3) is the Schrödinger equation with quasiperiodic potential $V(x) = V(x, qx+y)$ and energy $E = \hat{\omega}^2$. For a review of analytical results which will be useful in the following, see, for example, [18].

Before continuing with the general analysis we specify the explicit form of the function $V(x, qx+y) = \hat{V}(k_1 x, k_2 x)$ which will be used in the numerical computations below, namely

$$\begin{aligned} \hat{V}(k_1 x, k_2 x) &= \hat{V}_1(k_1 x) + \hat{V}_2(k_2 x) \\ &= -F \sum_{r=-\infty}^{+\infty} \delta(x - rL_1) - G \sum_{s=-\infty}^{+\infty} \delta(x - sL_2 + y/k_2)\,, \end{aligned} \tag{3.6}$$

where $L_i = 2\pi/k_i$, $i = 1, 2$, and $k_1 = 1$ and $k_2 = q$ are introduced for symmetry of notation. The δ-functions in the first and second sums contribute to V at $\theta_r = 0 \bmod 2\pi$, $\phi_r = 2\pi qr + y$ and $\phi_s = 0 \bmod 2\pi$, $\theta_s = 2\pi s/q - y/q$, respectively, with $r, s = 0, \pm 1, \cdots$, i.e. in two infinitely thin rings, the one toroidal with amplitude $-F$, and the other poloidal with amplitude $-G$.

Thus, F is a measure of how much modulation of the equilibrium there is in going around the poloidal way, and by analogy, G is a measure around the toroidal way. Therefore, large $|F|$ implies either large deviation from a circular cross-section (at large aspect ratio) and/or large poloidal variations ("inside – outside") induced by toroidicity (at small aspect ratio). Large $|G|$ implies strong deviation from axisymmetry of the torus.

This interpretation of F and G uses the declaration of θ and ϕ as poloidal and toroidal angles, respectively. There is nothing to prevent us, however, from reversing their rôles. In this case F, instead of G, is a measure of deviation from axisymmetry, etc. The safety factor q_s becomes $B^\theta/B^\phi = q^{-1}$. Thus, the rôles of F and G may be interchanged if q_s is replaced by q_s^{-1}. Indeed, since we varied F at constant G, we prefer this second possible nomenclature.

A δ-function model for V instead of a smooth function is chosen because it changes equ. (3.3) into a recursion, equ. (3.7) below. This permits much faster computation of solutions and spectra. Theory [18] shows that the general character of the spectrum of equ. (3.3) is the same for smooth V and a simple quasiperiodic δ-function series. For the particular potential (3.6) the same was made plausible in [19]. Methods (see below) of obtaining different components of the spectrum work for both types of potentials [19].

The differential equation (3.3) transforms to the recursion [19], [20], [21]

$$\begin{pmatrix} \hat{\omega}U_n \\ U'_n \end{pmatrix} = \begin{pmatrix} c_{n,n-1} & s_{n,n-1} \\ -s_{n,n-1} - c_{n,n-1}F_n/\hat{\omega} & c_{n,n-1} - s_{n,n-1}F_n/\hat{\omega} \end{pmatrix} \cdot \begin{pmatrix} \hat{\omega}U_{n-1} \\ U'_{n-1} \end{pmatrix} \quad (3.7)$$

from one pulse at $x = x_{n-1}$ to the next at $x = x_n$. Here $U_n = U(x_n + 0)$, $U'_n = \mathrm{d}U(x_n + 0)/\mathrm{d}x$, and $s_{n,m} = \sin[\hat{\omega}(x_n - x_m)]$, $c_{n,m} = \cos[\hat{\omega}(x_n - x_m)]$. F_n is either F or G, depending on what pulse is active. With equ. (3.6) the recursion for the pulses themselves is

$$x_n = \min\left\{ \left(\left[\frac{x_{n-1}}{L_1}\right] + 1 \right) L_1 , \left(\left[\frac{x_{n-1}}{L_2}\right] + 1 \right) L_2 \right\} , \quad (3.8)$$

where $[x]$ means the integer part of x. The field line parameter y has been made to zero for simplicity. This implies that a field line passing through $\theta = \phi = 0$ is investigated. Since all field lines come arbitrarily close to any point, this should not be a restriction; see [22].

After these preparations, both results from theory and numerical illustrations supporting the transition from global modes to ballooning-type modes are presented in the next section.

4. Global modes and ballooning-type modes

In the present context the following result proved in [23], [24] is relevant: equation (3.3) with quasiperiodic analytic potential $V(k_1x, k_2x)$ has solutions of the form

$$U(x) \;=\; \mathrm{e}^{i\alpha x}\; P(k_1x,\; k_2x) \;+\; c.c.\;, \tag{4.1}$$

where P is quasiperiodic in both arguments with period 2π, just as V is. This holds, provided $q = k_2/k_1$ is sufficiently irrational (diophantine condition) and $E = \hat{\omega}^2$ is sufficiently large ($E > E_0 = c(k_1, k_2)\max(V^2)$, c bounded) and provided E is not in an infinite set of gaps which may be labelled by two integers m, n. The coefficient α in the exponent and P are functions of E. At the edges of the gaps α assumes the values $(mk_1 + nk_2)/2$. (This is analogous to the periodic case; see, for example, the Mathieu equation where $k_2 \equiv 0$, in [25].) This implies the existence of global (Alfvén) solutions if m and n are even: U becomes $U = U_{m,n}(x) = \exp[i(mk_1 + nk_2)/2]\, P(k_1x, k_2x)$ and this has the right double periodicity to fit onto the torus. Thus, although the solution is constructed along an ergodic field line, it fits together smoothly across the windings on the whole surface.

The fact that there is a lower bound E_0 is an indication that different phenomena may be at work if, at fixed E, the amplitudes F, G in V are sufficiently increased. This will be discussed below. For later purposes we also note that in spite of the infinitely many gaps present those values of E for which α is real constitute a continuous spectrum σ_c of equ. (3.3) [23], [24].

In order to find the global solutions, it is necessary to locate the gaps first. There are several possibilities. One can simply run equ. (3.3), i.e. the recursion (3.7), forward from some arbitrary initial condition. In the gaps U goes to infinity exponentially fast [18] (or to zero; but this is numerically unstable and ends up in a growing branch, too [19]). Outside the gaps, according to equ. (4.1), U stays bounded. A working definition of runaway is, for example, an amplitude $A = \sqrt{\hat{\omega}^2U^2 + U'^2}$ larger than $A_0 = 10^5$ after at most $N = 10^4$ iterations. As an example, the upper trace of Fig. 1 is obtained. It shows the region $E = 0.145 - 0.180$. At intervals $\delta E = 4.375 \cdot 10^{-5}$, bounded solutions are marked with a dot and exploding ones are left blank. Several gaps are evident at this resolution. Higher resolution would reveal finer and finer gaps. Figure 1 is made with amplitudes $F = 0.4$ and $G = 0.8$. As in all figures shown, $k_1 = 1$ and $k_2 = q = (\sqrt{5} - 1)/2$ are assumed.

Another possibility to locate the gaps which avoids dealing with large numbers and

their potentially negative effects on numerical accuracy is the following: let an angle Φ and a winding number w be defined by $\tan\Phi = \hat{\omega}U/U'$ and $w = \lim_{x\to\infty}\Phi(x)/x$. According to [18], [26], the winding number is a nondecreasing continuous function of E of the devil's staircase type. It has plateaus on which w is constant and assumes the values $w = (mk_1 + nk_2)/2$, with $m,\ n = 0,\ \pm1,\ \pm2,\ \cdots$. The gaps for $E > E_0$ mentioned before coincide with plateaus of w. Φ satisfies the equation $\Phi' = \hat{\omega} - (V/\hat{\omega})\sin^2\Phi$ or the corresponding recursion in the case of δ-function potentials [19]. By running it long enough, say for $N = 10^4$ iterations, one obtains w. The middle trace in Fig. 1 shows $w(E)$ thus obtained at the same points as in the trace above. Some of the plateau indices (m,n) are indicated. In the region shown the gaps and the plateaus agree. We shall return to the complement of the plateaus of $w(E)$ below.

At the edges of the gaps there exists a second linearly independent and *secular* solution U, in addition to the desired quasiperiodic one. It can be avoided by selecting the initial value Φ_0 of $\Phi = \arctan(\hat{\omega}U/U')$ properly. (For this purpose and the exact localization of an edge quite a bit of fine tuning is required.)

As a result one obtains the global Alfvén modes as shown in Figs. 2 to 5. In the figures $U(\theta,\phi)$ is given as a function of ϕ or θ alone, with the complementary variable kept constant. All figures correspond to the left boundary of the same gap, $(m,n) = (6,-8)$. In Fig. 1 this gap is just barely visible. From the two amplitudes F and G, which determine the "geometry", G is kept fixed arbitrarily at $G = 0.8$, as in all subsequent figures too, while F increases from zero to 0.57. For brevity, we call this parameter F "nonaxisymmetry"; see Sec. 3. The scale of the figures is always the same. $U(\theta = 0, \phi = 0)$ has been chosen as $(\sin\Phi_0)/\hat{\omega}$, which does not vary much from figure to figure.

Figure 2 shows the axisymmetric case $F = 0$. From comparison with Fig. 3 it is evident that a small amount of nonaxisymmetry ($F = 0.3$) does not change the Alfvén mode much. Elevated levels of nonaxisymmetry ($F = 0.5$, Fig. 4) add higher Fourier harmonics. Also, the number of local maxima and minima increases, with a few of them dominating the others. This tendency continues with increasing F. At $F = 0.57$, finally (see Fig. 5), the dependence on θ and ϕ has become quite rough. There are extrema with very steep gradients. Shortly above this value of F, at F_0 somewhere in the range $0.57 < F_0 < 0.6$, Alfvén modes with $(m,n) = (6,-8)$ cease to exist.

In agreement with the definition of the winding number it can be observed in Figs. 2 to 5 that the number of nodes in the variables θ and ϕ, namely 6 and 8, remains constant and agrees with $|m|$ and $|n|$, respectively. Alfvén modes in nonaxisymmetric toroidal

geometry can therefore be uniquely labelled by their poloidal and toroidal node numbers. (More precisely, as with sin and cos there is a *pair* of modes (m, n), corresponding to the two ends of each gap.) A global Alfvén mode has already been found for a related δ-function potential in [22], but its evolution as a function of nonaxisymmetry has not been considered.

The figures just described correspond to behaviour on toroidal and poloidal cuts $\theta = 0$ and $\phi = 0$, respectively. It is straightforward to obtain the solution analytically at other positions along the field line if it is known on the cuts, since $V \equiv 0$ in equ. (3.3) between the pulses. If one wants to obtain $U(\theta, \phi)$ on a regular θ, ϕ grid, however, as is required by most 3-d graphics packages, some interpolation is necessary. We run the iteration (3.7) a few thousand times in order to have a dense set of values on the cuts, and then follow the solution from a desired grid point back to the closest available point on the cuts. In this way the 3-d visualizations of $U(\theta, \phi)$, Figs. 6 to 9, are obtained. They belong to the same parameters as Figs. 2 to 5, respectively. The ϕ-domain was shifted from $(0, 2\pi)$ to $(-\pi, \pi)$ in order to bring out the structure more clearly.

A smooth transition from axisymmetry to weak nonaxisymmetry is again evident. With increasing nonaxisymmetry an "inflation-type" structure develops in the middle of the figure. (It should be remembered, however, that the figures do not show a radial displacement but a component of $\boldsymbol{\xi}$ *within* a resonant surface.) With the approach to the breakdown of the mode this structure becomes dominant. It separates into parallel ridges of shrinking lateral extent. Analysis shows that the direction of the crests and valleys in the figures is always along the field line.

What happens for nonaxisymmetry $F > F_0$ can be found out by resorting again to the theory of the quasiperiodic Schrödinger equation [18], [26]. It has been proved that equ. (3.3), for almost all potentials, has not only a continuous spectrum σ_c, but also a dense spectrum of point eigenvalues, σ_p. The corresponding eigenfunctions $U(x)$ fall off asymptotically for $x \to \pm\infty$ along the field line as $\exp(-|x|/L)$, i.e. with a finite decay length $L(E)$. Owing to this property an eigenmode from σ_p does not fit together any more into a global (Alfvén) mode with double periodicity condition on the ergodic surface. Instead, the mode is infinitely thin across the field line and its amplitude is negligibly small almost everywhere: only along a finite section of order $2L$ along the field line is $U(x)$ appreciably different from zero. In other words, *eigenmodes* of equ. (3.3) are of the (Alfvén) *ballooning* type, as introduced in Sec. 2. The dense set of eigenvalues corresponds to a dense set of positions of the maxima along the field line and to a dense set of decay lengths L.

Before methods to obtain the point spectrum and the eigenfunctions are discussed, it is useful to give an example. Figures 10 and 11 show a typical eigenmode. In Fig. 10 the amplitude $A_1(n) = \sqrt{\hat{\omega}^2 U^2 + U'^2}$ is plotted logarithmically along the field line at cuts $\theta = 0$ as a function of the number n of cut crossings. An exponential decay, on the average, on both sides of a peak, interrupted at low level by a submaximum, is evident. The parameters are $F = 0.7$ and $E = 0.12128$.

Figure 11 gives an impression of the eigenmode as a function of θ and ϕ on the surface, albeit, owing to the peculiarity of the plot program, a somewhat poor one. Indeed, as theory predicts, there are "infinitely" thin ridges (and troughs) going around the torus a few times along the field line and then becoming negligibly small. (The needles are just an artefact: the ridges have an exceedingly small chance of being intercepted by the discrete assembly of N_g grid points. Even with $N_g = 200 \times 200$ in Fig. 11, compared with $N_g = 100 \times 100$ in the previous figures, there are always grid points which miss the ridges. This cuts the continuous structure into pieces, visible as needles. Their finite thickness is also an artefact: In order to increase the chance of "detection" on the grid, the interpolation of the solution on the boundaries has deliberately been made coarse.) Eigenmodes with other values of E are qualitatively similar to Figs. 10 and 11. Details, such as the positions of the ridges in the θ, ϕ plane, etc. are of course different from case to case.

The value of E in Figs. 10 and 11 is peculiar, however, since, at the amplitude $F = 0.7$, it represents the "successor" case to the global modes in Figs. 2 to 9. It was selected from a set of available eigenvalues (see below) because its winding number is again close to the left boundary of the (6,-8) plateau.

The comparison of the Alfvén mode from Fig. 9 and the Alfvén ballooning mode from Fig. 11 shows how the transition between the two types of modes takes places when the nonaxisymmetry exceeds the critical value F_0: ridges already present in the Alfvén mode become infinitely steep. At the same time the global smooth coherence of the solution is lost.

Eigenmodes of equ. (3.3) or its discrete version, equ. (3.7), as just described in an example, cannot be found by running the equations forward in time. It has been shown in [19] that this method is numerically unstable for modes from the point spectrum. A boundary method, however, works well [19]. For the recursion (3.7), for example, one can set $U_{n=0} = U_{n=N+1} = 0$ for some large number N and apply the normalization $\sum_{n=1}^{N} U_n^2 = 1$. This gives $N + 1$ equations for the $N + 1$ unknowns $U_1, \cdots U_N$, E. A nonlinear-equation solver with some trial function converges in the majority of cases

to an eigenvalue E and an eigenfunction with exponential decay on both sides of a maximum. This is how the mode in Figs. 10 and 11 was obtained, with $N = 400$.

Although one can easily obtain a handful of eigenvalues and eigenfunctions in this way, by using different trial functions, the method is unsuited to a systematic study of the point spectrum. For this purpose several other methods are available. The simplest way, in principle, is to look for zeros of the determinant d of the homogeneous recursion equations (3.7). With the boundary conditions mentioned above the corresponding matrix is tridiagonal. Special care is required, however, owing to the presence of poles in the function $d(E)$ [19].

Another method is furnished again by the theory of the quasiperiodic Schrödinger equation [18], [26]. It states that the total spectrum (continuous, σ_c, and point spectrum, σ_p,) consists of those values of E for which the winding number $w(E)$ is not a constant. For an E thus obtained, membership in σ_c or σ_p can be discriminated by evaluation of the Lyapunov exponent $\Lambda_\Phi = \lim_{x\to\infty}(\ln|\delta\Phi/\delta\Phi_0|)/x$. Here $\delta\Phi$ is a small perturbation of the angle Φ. A recursion for $\delta\Phi_n$ is easily derived from the recursion for Φ_n itself [19]. It can be shown [19], [27] that $\Lambda_\Phi = 0$ for modes in the continuous spectrum, while $\Lambda_\Phi \neq 0$ for the point spectrum.

The function $\Lambda_\Phi(E)$ is shown in Figs. 1 and 12. In Fig. 1, at amplitude $F = 0.4$, Λ_Φ is zero wherever $w(E) \neq$ const. In contrast, in Fig. 12, with very large amplitude $F = 0.7$, Λ_Φ differs from zero also at $w(E) \neq$ const. This indicates the presence of a pure point spectrum σ_p in the parameter region $E = 0.115 - 0.150$ shown (apart from gaps). Figures 10 and 11 are an example taken from this region. As expected, the continuous spectrum (upper trace) is empty in Fig. 12.

Figure 13, finally, gives an overview of the spectral behaviour of equs. (3.3), (3.6) for nonaxisymmetry F ranging from -1.0 to $+1.0$, at fixed $G = 0.8$, in the region $E = \hat{\omega}^2 = 0. - 1.0$. The continuous spectrum is again marked by dots (merging into lines), while point eigenvalues are marked by vertical bars. The numerical criterion used for $E = r \cdot \delta E$ ($r = 0,\ 1,\ \cdots\ 1000,\ \delta E = 10^{-3}$) to be in σ_p was $|\Lambda_\Phi| > a_1 = 2 \cdot 10^{-3}$ and $|\delta w| > a_2 = 10^{-3}$, where δw is the biggest difference in $w(E)$ of a point E to its nearest neighbours $E \pm \delta E$. The choices of a_1, a_2 and δE contain some arbitrariness leading to a few possibly wrong allocations. Of course, only the most prominent gaps remain visible on this scale. Nevertheless, from Fig. 13 and from extending $|F|$ to even higher values one obtains the result: at fixed eigenvalue parameter E or at fixed winding number w any mode from the continuum of equs. (3.3), (3.6) transforms to a localized eigenmode if the nonaxisymmetry $|F|$ is raised above a critical threshold.

The lower left corner of Fig. 13 is particularly densely covered by point eigenvalues. The reason for this effect is discussed in the Appendix.

5. Discussion and conclusions

Axisymmetric toroidal plasmas exhibit Alfvén modes, which are singular across the resonant ψ surfaces [3], [6], and ballooning modes (proper), which are singular across field lines, and have the displacement vector $\boldsymbol{\xi}$ and magnetic field perturbation $\mathbf{b}$ pointing out of the ψ surface; see [10] for ergodic field lines, as considered here. From a mathematical point of view the former belong to a continuous spectrum, while the latter belong to a dense point spectrum.

A plasma model was devised which allows simple numerical analysis of the spectrum and modes in the *nonaxisymmetric* case, too. Analytical results from the theory of the quasiperiodic Schrödinger equation [18] were used as guidelines. Additional evidence exists that more general quasiperiodic equations have similar properties [27].

The following results were obtained: Alfvén modes continue to exist in nonaxisymmetry. They come in pairs which may be uniquely labelled by their node numbers (m, n) on poloidal and toroidal cuts. At fixed (m, n) there is a critical amount of nonaxisymmetry, or, at given nonaxisymmetry, a critical amount of poloidal modulation above which the Alfvén mode contracts within the surface and becomes an infinitely thin *Alfvén ballooning* mode. These modes have the displacement vector $\boldsymbol{\xi}$ and field perturbation $\mathbf{b}$ *within* the resonant ψ surface. Alfvén ballooning modes also have a dense point spectrum. In contrast to ballooning modes proper, they do not exist in the axisymmmetric case. The reason for this difference is the following: ballooning modes proper having a normal component of $\boldsymbol{\xi}$ and $\mathbf{b}$ feel the effect of shear, which moves two initially close field lines on neighbouring ψ surfaces apart. This deteriorates the resonance and gives a natural cut-off length along the field line on both sides of a resonant region. Alfvén balloonings, on the other hand, owing to their polarization, do not feel shear. In axisymmetry perturbations experience a periodical modulation of the background along the field line. According to Floquet theory, in this situation modes can fall off to one side or the other only, but not on both sides simultaneously. Hence no Alfvén ballooning eigenmodes can form in axisymmetry.

Alfvén ballooning modes are stable. This follows from a straightforward modification of the stability proof for global Alfvén modes as given in, for example, [7], [8]. The integration over a resonant surface there has to be replaced by integration along

a field line and periodicity conditions have to be replaced by the condition that the mode amplitude vanish asymptotically at $s \to \pm\infty$.

The assumption used above that a nonaxisymmetric toroidal MHD equilibrium exists does not seem to be fundamental to our conclusions. With appropriate modifications, they should still be valid for a nonideal equilibrium provided constant-pressure surfaces with field lines going around the torus many times still exist.

Appendix

The average value $\langle V \rangle$ of the potential V, according to equ. (3.6), is $\langle V \rangle = \langle \hat{V}_1 \rangle + \langle \hat{V}_2 \rangle = -F/L_1 - G/L_2$. With a potential $\tilde{V} = V - \langle V \rangle$ defined such that its average value is zero, equ. (3.3) can be written as

$$\left[\frac{\mathrm{d}^2}{\mathrm{d}x^2} + (E_{\mathrm{eff}} - \tilde{V}) \right] U(x) = 0 , \tag{A.1}$$

where

$$E_{\mathrm{eff}} = E + F / L_1 + G / L_2 \tag{A.2}$$

is now the effective eigenvalue parameter. In a simplified picture disregarding the presence of multiple potential troughs and hills, one would expect to see a "bound state" ($U^2(x)$ decreasing exponentially on both sides outside a potential trough) provided $E_{\mathrm{eff}} < 0$. Troughs exist for $G > 0$ and/or $F > 0$, while $E_{\mathrm{eff}} < 0$ (at $E \geq 0$) requires $F < 0$ and/or $G < 0$. At $G = 0.8$ this is compatible on the left of the dashed line $E_{\mathrm{eff}} = 0$ in Fig. 13. Indeed, this region is filled with point eigenfunctions. Such a simple interpretation of eigenfunctions is not possible in the rest of the parameter space. Interference over distances covering many potential troughs and hills together plays a decisive role there.

For more realistic functions $V(x)$ defined by equs. (3.2), (3.5) it remains to be seen under what conditions $E_{\mathrm{eff}} < 0$ is possible.

References

[1] J.P. Freidberg, *Ideal Magnetohydrodynamics* (Plenum Press, New York, NY) 1987.

[2] K. Appert, R. Gruber and J. Vaclavik, Phys. Fluids 17, 1471 (1974).

[3] J. P. Goedbloed, Phys. Fluids 18, 1258 (1975).

[4] W. Grossmann and J. Tataronis, Z. Physik 261, 217 (1973).

[5] R. Cairns, *Radiofrequency Heating of Plasmas* (Hilger, Bristol) 1991.

[6] Y.P. Pao, Nucl. Fusion 15, 631 (1975).

[7] J.A. Tataronis, J.N. Talmadge and J.L. Shohet, University of Wisconsin Report ECE - 78 - 10 (1978) and Comments Plasma Phys. Controlled Fusion 7, 29 (1982).

[8] J.A. Tataronis and A. Salat, Courant Inst. Report MF - 98; DOE/ER/03077-171 (1981) and E. Canobbio, H.P. Eubank, G.G. Leotta et al. (Eds.) *Heating in Toroidal Plasmas* Proc. 2nd Joint Grenoble - Varenna Int. Symp., Como, Italy (1980), Vol. II, p.655, EUR-7424 EN (1981).

[9] R.L. Dewar and A.H. Glasser, Phys. Fluids 26, 3038 (1983).

[10] E. Hameiri, Commun. Pure and Appl. Math. XXXVIII, 43 (1985).

[11] E. Hameiri, Phys. Fluids 24, 562 (1981).

[12] T. Kato, *Perturbation Theory for Linear Operators* (Springer, New York, NY) 1976.

[13] J.W. Connor, R.J. Hastie and J.B. Taylor Proc. R. Soc. London A. 365, 1 (1979).

[14] D. Correa-Restrepo, Z. Naturf. 33a, 789 (1978).

[15] G.O. Spies, Nuclear Fusion 19, 1532 (1979).

[16] J.M. Greene and J.L. Johnson, Phys. Fluids 5, 510 (1962).

[17] M.P. Bernardin and J.A. Tataronis, Phys. Fluids 27, 133 (1984).

[18] B. Simon, Advances Appl. Math. 3, 463 (1982).

[19] A. Salat, Phys. Rev. A, to be published, and Report IPP 6/298 (1991).

[20] J.B. Sokoloff and J.V. José, Phys. Rev. Lett. 49, 334 (1982).

[21] J. Bellisard, A. Formoso, R. Lima et al., Phys. Rev. B 26, 3024 (1982).

[22] A. Salat, Z. Naturf. 37a, 830 (1982).

[23] E.I. Dinaburg and Ya.G. Sinai, Funct. Anal. Appl. 9, 279 (1976).

[24] H. Rüssmann, Ann. N.Y. Acad. Sci. 357, 90 (1980).

[25] M. Abramowitz and I.A. Stegun, Eds., *Handbook of Mathematical Functions*, p. 721, (National Bureau of Standards, Washington, D.C.) 1968.

[26] R. Johnson and J. Moser, Commun. Math. Phys. 84, 403 (1982).

[27] F.J. Romeiras, A. Bondeson, E. Ott et al., Physica 26D, 277 (1987).

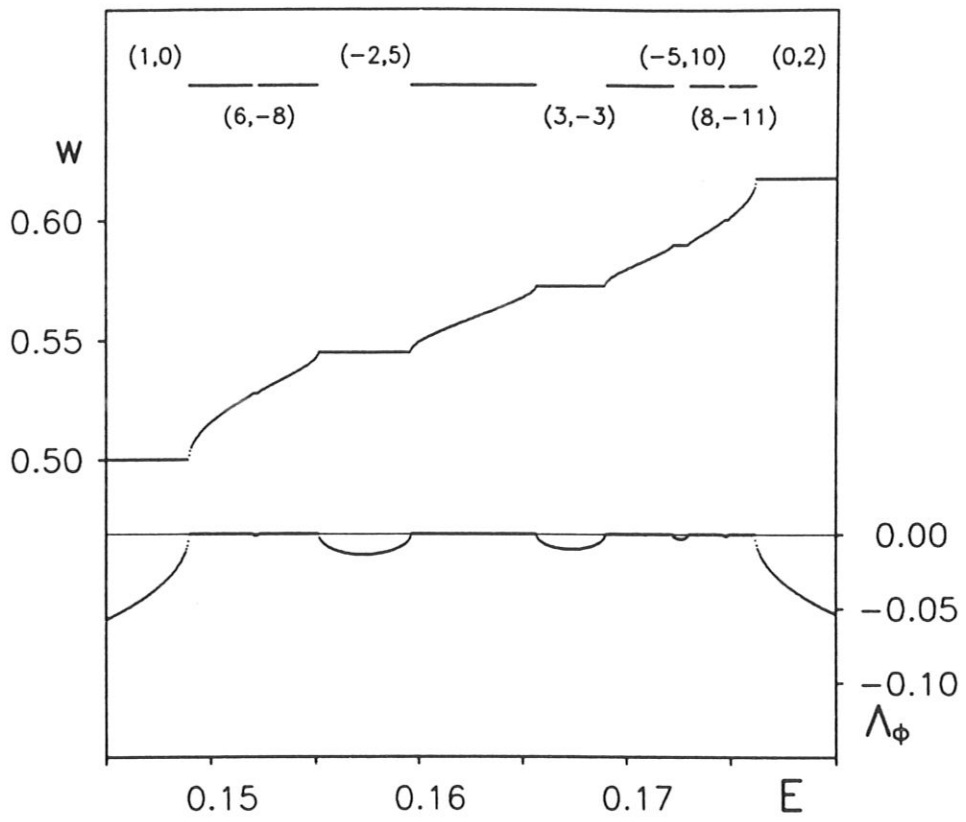

Figure 1: Upper trace: continuous spectrum of equs. (3.3), (3.6) as a function of the eigenvalue parameter $E = \hat{\omega}^2$. Middle trace: winding number $w(E)$. Pairs of numbers (m, n) specify $w = (m\,k_1 + n\,k_2)/2$ in some prominent plateaus. Lower trace: Lyapunov number $\Lambda_\Phi(E)$. ($F = 0.4,\ G = 0.8$).

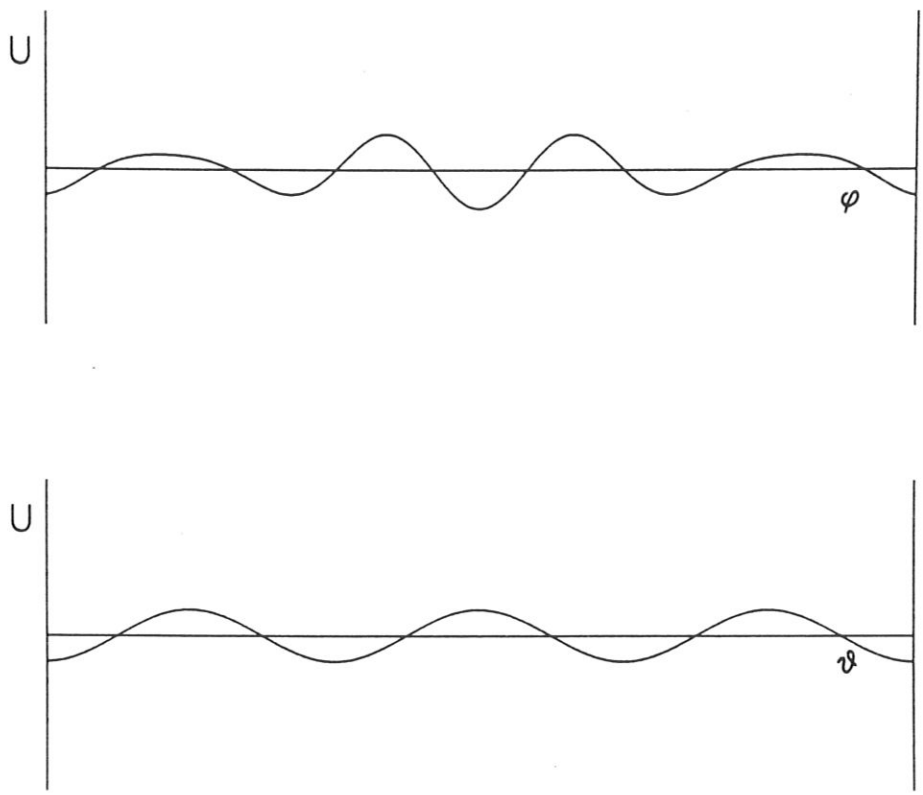

Figure 2: Alfvén solution $U(\theta, \phi)$. Upper part: at fixed θ; lower part: at fixed ϕ. $G = 0.8$. Axisymmetric case: $F = 0$. ($E = 0.19034$, $\Phi_0 = -0.26\,\pi$).

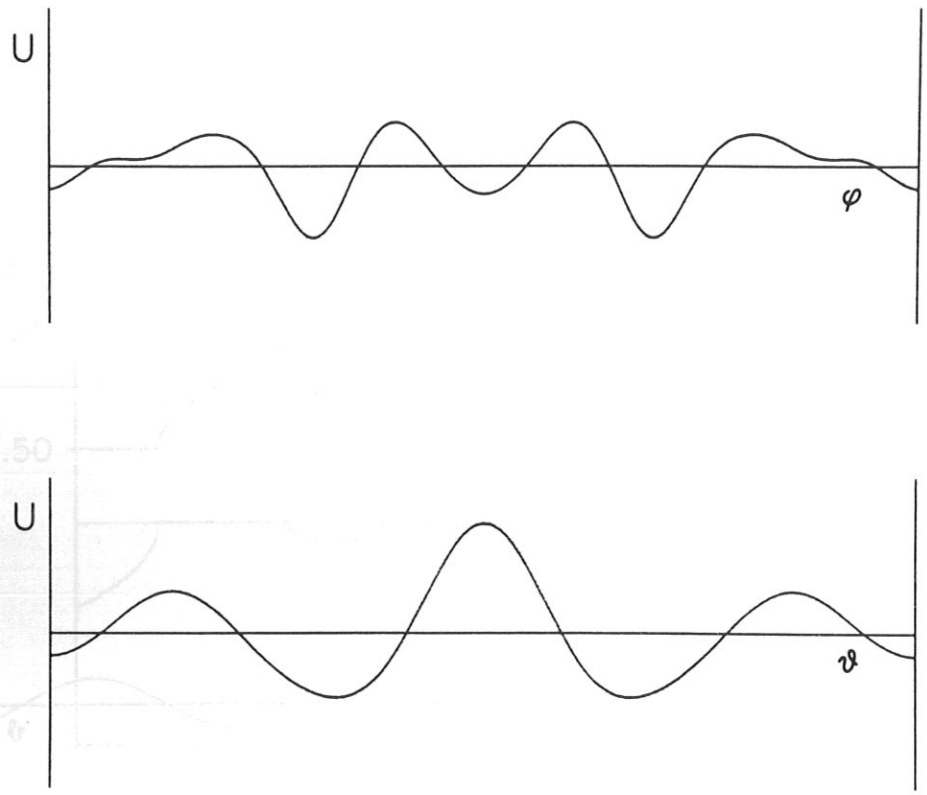

Figure 3: Same as Fig. 2. Case with small nonaxisymmetry: $F = 0.3$. ($E = 0.160099,\ \Phi_0 = -0.2035\,\pi$).

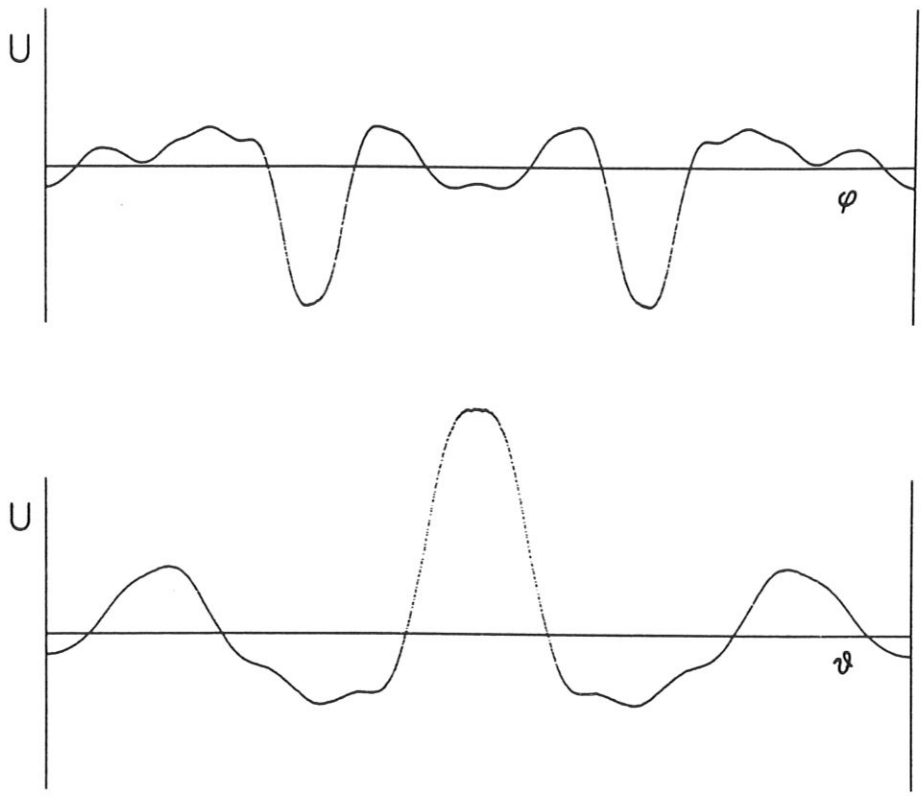

Figure 4: Same as Fig. 2. Case with medium nonaxisymmetry: $F = 0.5$. ($E = 0.14291363,\ \Phi_0 = -0.16784\,\pi$).

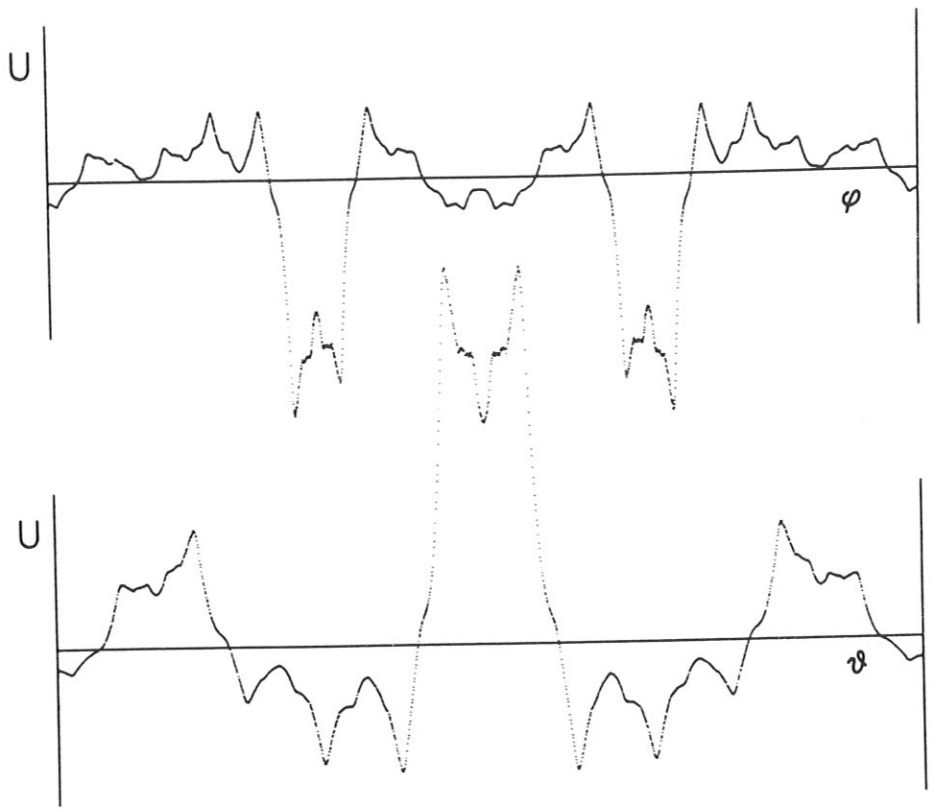

Figure 5: Same as Fig. 2. Case with large nonaxisymmetry: $F = 0.57$. ($E = 0.13571937,\ \Phi_0 = -0.15718\,\pi$).

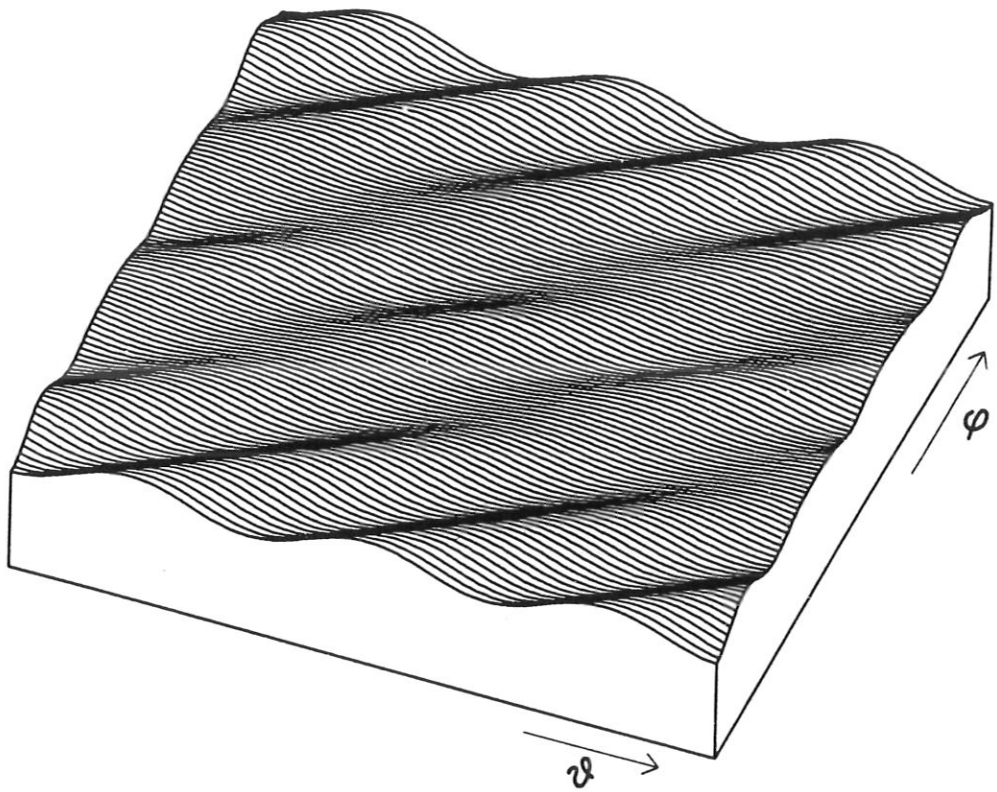

Figure 6: Alfvén solution $U(\theta, \phi)$. Parameters as in Fig. 2.

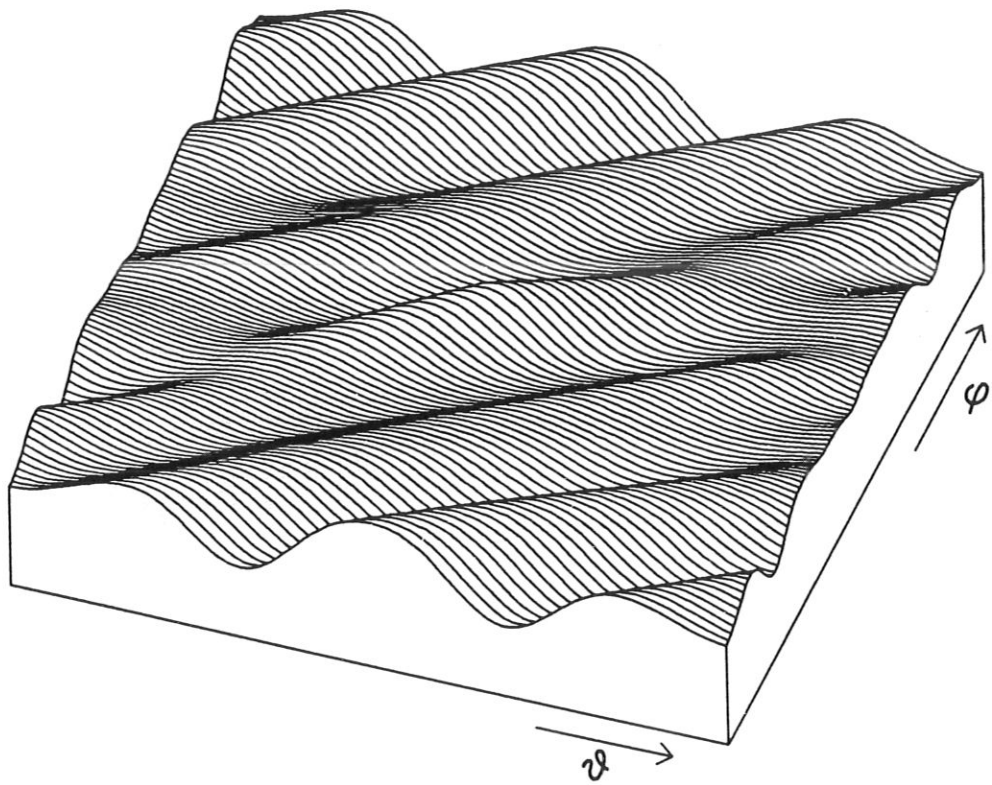

Figure 7: Alfvén solution $U(\theta, \phi)$. Parameters as in Fig. 3.

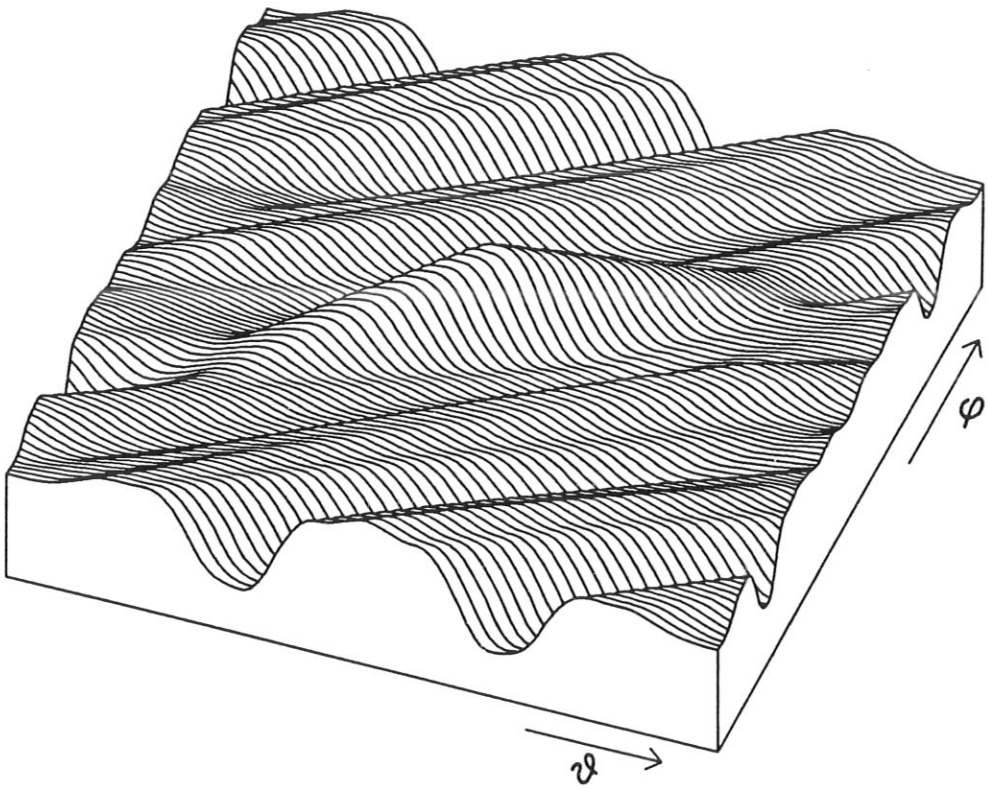

Figure 8: Alfvén solution $U(\theta, \phi)$. Parameters as in Fig. 4.

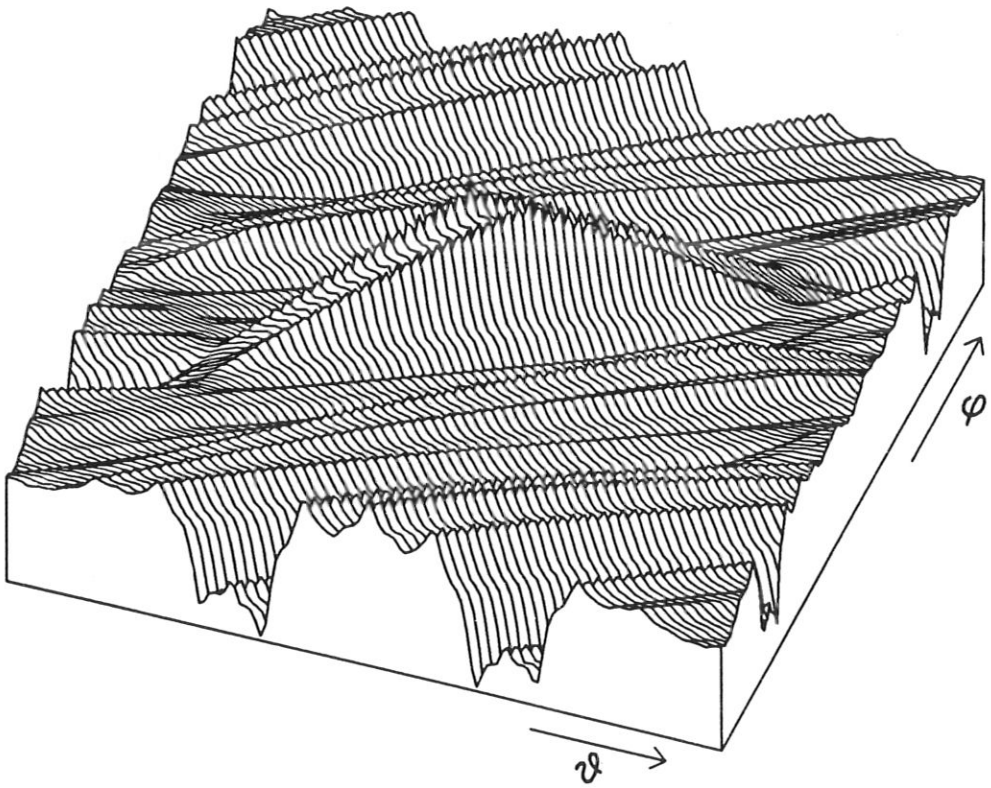

Figure 9: Alfvén solution $U(\theta, \phi)$. Parameters as in Fig. 5.

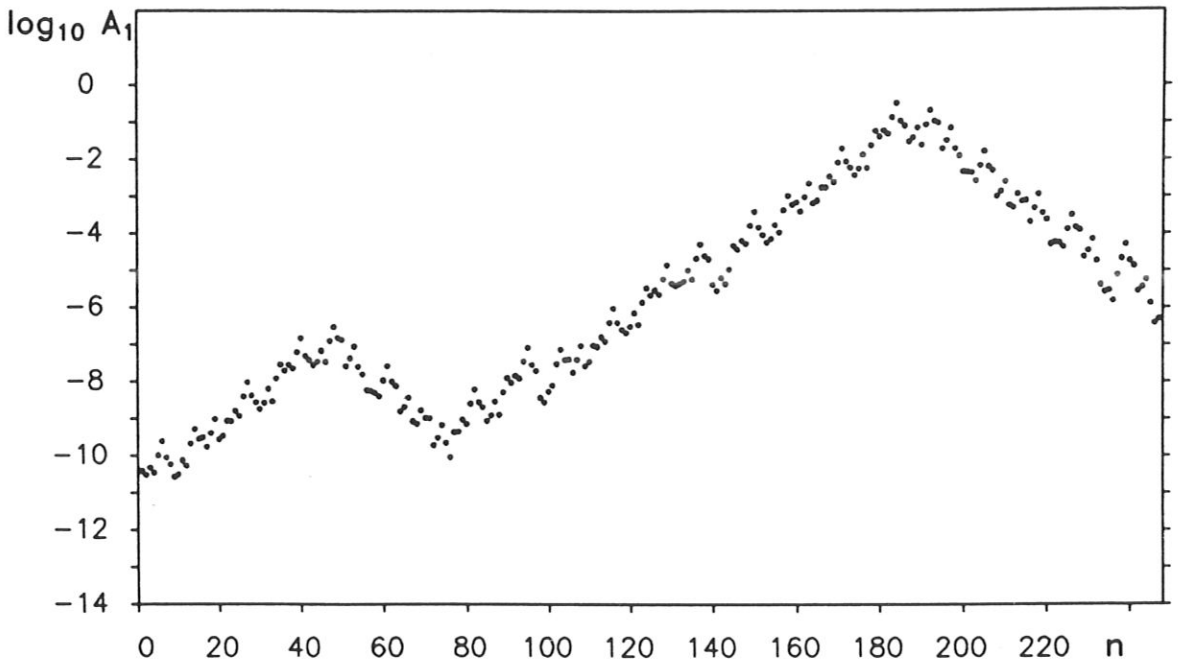

Figure 10: Amplitude $A_1(n) = \sqrt{\hat{\omega}^2 U^2 + U'^2}$ of ballooning solution along the field line at successive poloidal cuts. $F = 0.7$. $(E = 0.12128)$.

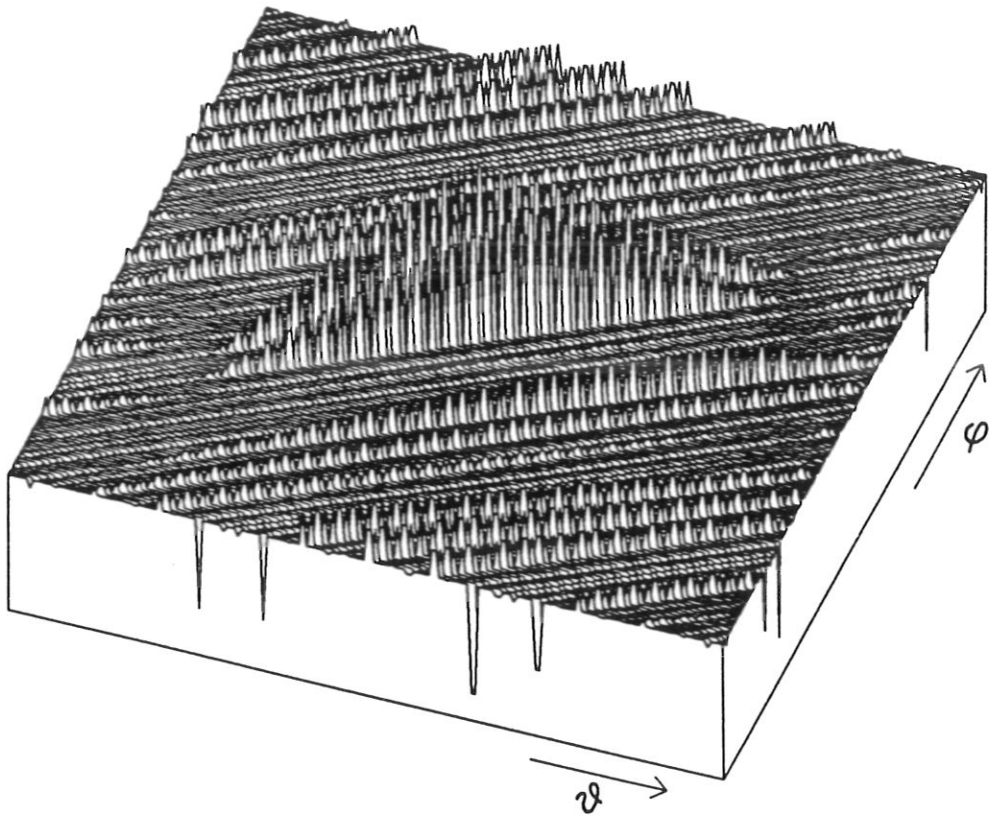

Figure 11: Alfvén ballooning solution $U(\theta, \phi)$. Chains of needles instead of continuous ridges are an artefact of the coarse grid. Case with very large nonaxisymmetry: $F = 0.7$. $(E = 0.12128)$.

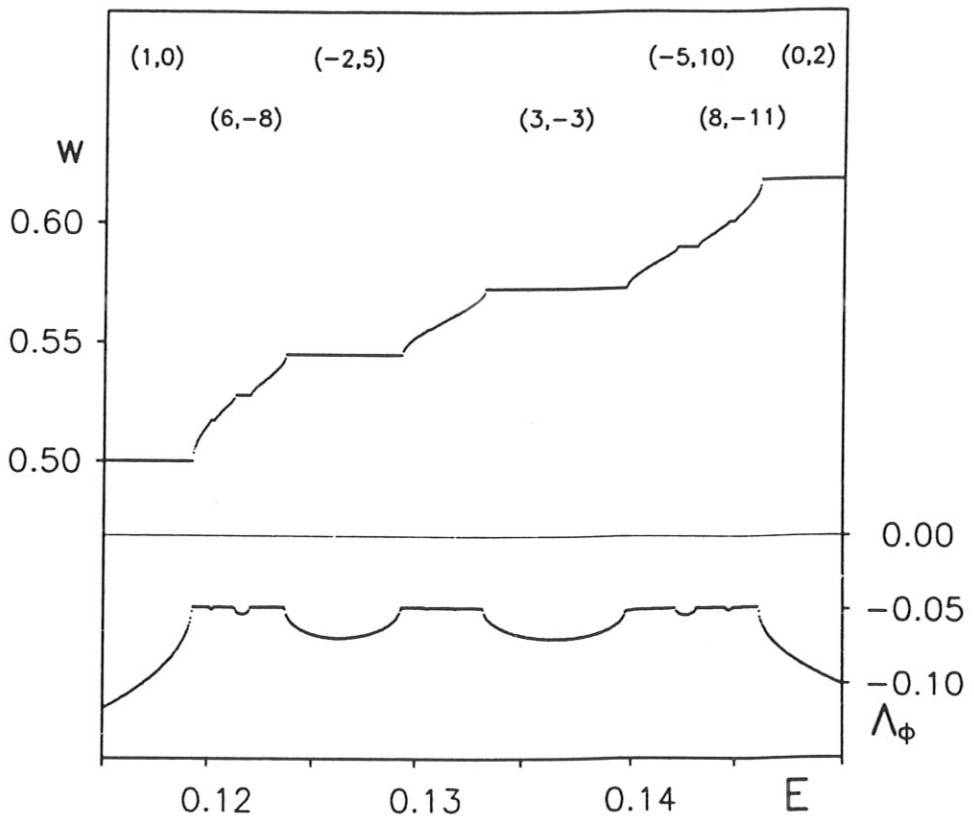

Figure 12: Same as Fig. 1. Case with very large nonaxisymmetry: $F = 0.7$. The continuous spectrum is empty.

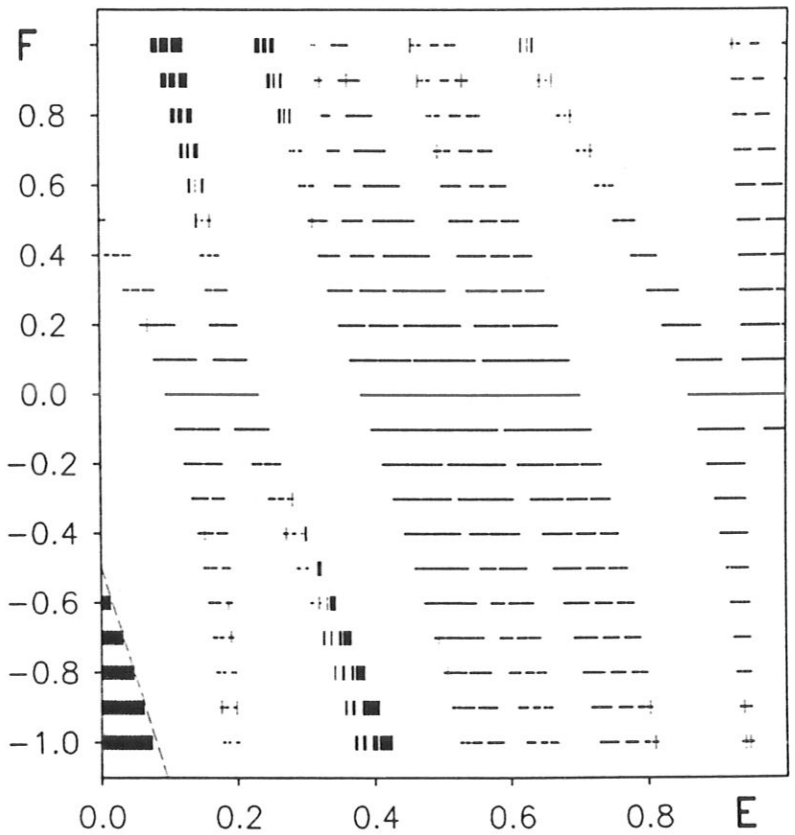

Figure 13: Overview of the spectrum of equ. (3.3) for different non-axisymmetries F. Continuous spectrum: dots. Point spectrum: bars. Dashed line: $E_{\text{eff}} = 0$. To its left: $E_{\text{eff}} < 0$ in the presence of potential troughs.